

Localizing Contour Points for Indexing an X-ray Image Retrieval System

Xiaoqian Xu^a, D. J. Lee^{*a}, S. Antani^b, and L. R. Long^b

^aDept. of Electrical and Computer Eng., Brigham Young University, Provo, UT 84602

^bNational Library of Medicine, Bethesda, MD 20894

xiaoqian@et.byu.edu, djlee@ee.byu.edu, antani@lhcnlm.nih.gov, and
long@lhcnlm.nih.gov

Abstract

Vertebra shape can effectively describe various pathologies found in spine x-ray images. There are some critical regions on the shape contour which help determine whether the shape is pathologic or normal. We selected a subset of 250 segmented vertebra boundaries for study from a collection of 17,000 digitized x-rays of cervical and lumbar spine taken as a part of the second National Health and Nutrition Examination Survey (NHANES II). A board certified expert radiologist marked nine morphometric landmark points on the contour of these cervical and lumbar images. Image indexing could mimic the model used by the radiologists to mark the images, e.g. 6-, 9-, or 10-point, thereby improve the query and retrieval of vertebra shapes from the image database. In this paper, we present a technique to automatically select nine points from the boundary contour. The comparison between two 9-point models using the L_2 distance and retrieval rank results derived respectively from the 9-point model marked by the expert and the 9-point model selected with our algorithm provides a good measure of how well the two models match.

1. Introduction

There has been growing interest in indexing images with biomedical content, especially in developing an automated or computer-aided retrieval system. Image matching schemes based on grayscale image distance correlation are too computationally expensive and too sensitive to the image contrast and noise and are not meaningful for x-ray image retrieval. Shape-based retrieval techniques show a great potential for this task although it's still very challenging because of highly similar shape properties [1-4]. In this research, the focus is on locating nine anatomy relevant contour points that match closely with the 9-point model used by the expert for image retrieval ranking.

For medical images, shape is one of the important features that effectively describes various pathologies identified by medical experts. Several other models are also used by radiologists to mark significant points on the vertebra boundary, viz. 6-, 8-, 10-point models [5]. For the cervical and lumbar x-ray images, the expert radiologists selected the 9-point model to mark critical points on the shape, which provide sufficient information for diagnosis. These nine points have the semantic relevance as follows:

Points 1 and 4 mark the upper and lower posterior corners of the vertebra, respectively;

Points 3 and 6 mark the upper and lower anterior corners of the vertebra, respectively;

Points 2 and 5 are the median along the upper and lower vertebra edge in the sagittal view;

Point 7 is the median along the anterior vertical edge of the vertebra in the sagittal view; Points 8 and 9 mark the upper and lower anterior osteophytes; if osteophyte(s) are not present on the vertebra, then these points coincide with points 3 and 6, respectively. Figure 1 shows two examples of the selections of these points and their overlays with the original image.

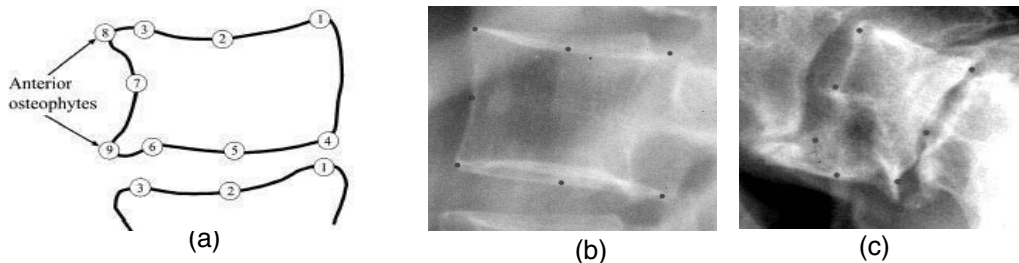


Figure 1. (a) Radiologist marked 9 points on the shape, (b) 7 points, and (c) 9 points

2. Algorithms

2.1. Shape acquisition and pre-processing

Shape extraction of x-ray images is a challenging task due to low image contrast. The contour of a cervical or lumbar x-ray image may not have a thin edge, which means for each image, we may detect an inside and an outside contour that are not the same. There actually is an annular area between them. The 9 points marked by the radiologist may not coincide with those extracted automatically from the boundary contour. However, the extracted nine points can still maintain the same relative positions as the marked 9 points. Since the indexing is based on a translation invariant similarity measure, the shift in these nine points will not affect the indexing results.

For each of the subset of 250 vertebral images, 40 points were extracted using Active Contour Models [6-7]. Although these 40 points contain accurate shape information similar to the original x-ray image contour, the number of contour points must be increased for selecting the nine points. The smooth contour makes the selection of nine points more flexible and reliable. Cubic spline curve interpolation was applied to the 40 points as the pre-processing. Cubic spline curve interpolation provides a smoother contour that is much closer to the original one. The number of points on the contour after interpolation is about 200, depending on the perimeter. Figure 2 shows how the interpolated contours and the x-ray images match. X-ray_1 has all 9 points marked (with osteophytes) and X-ray_2 has only 7 points (without osteophytes).

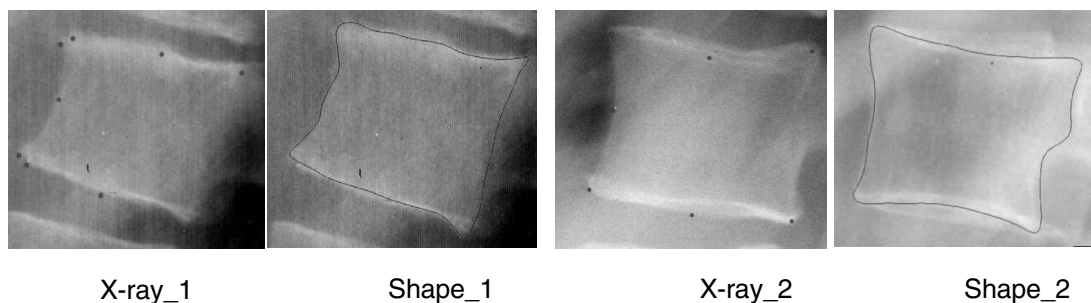


Figure 2. Shape_1 matches X-ray_1 and Shape_2 matches X-ray_2

2.2. Nine-point auto selection

Following the semantic relevance of nine points described above, points 1, 3, 4 and 6 are either the upper or the lower corners of the vertebra. The corners are the most significant shape features in this case. So, curve evolution technique [8-9] that eliminates insignificant shape features was implemented to reduce the number of data points while keeping the most significant ones. Curve evolution simplifies the contours by removing vertices with irrelevant shape features. This is achieved by iteratively comparing the relevance measure of all remaining vertices on the polygon. A relevance measure was developed to remove vertices with short and straight neighboring line segments. It can be expressed in Equation 1 as:

$$K(s_1, s_2) = \frac{|\beta(s_1, s_2) - 180| l(s_1) l(s_2)}{l(s_1) + l(s_2)} \quad \text{Equation 1}$$

, where $\beta(s_1, s_2)$ is the angle between two line segments s_1 and s_2 and $l(s_1)$ and $l(s_2)$ represent the normalized length (to the total length) of s_1 and s_2 , respectively. Higher relevance value means that the vertex has larger contribution to the shape of the curve. The angle $\beta(s_1, s_2)$ was calculated as the outer angle between two line segments. Both the angle and the length contribute to the relevance measure in the curve evolution process as shown in Equation 1. The curve evolution was stopped when the number of remaining vertices was down to 20 as shown in Figure 3. The bend angle was then calculated for each of those 20 points and it's calculated so that the clockwise turn gives a negative angle whereas a counter clockwise turn gives a positive angle.

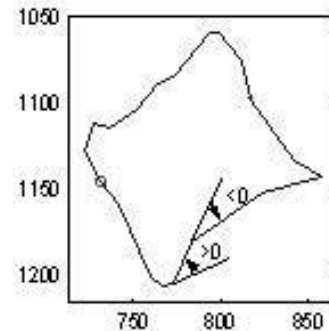


Figure 3. Bend angle

Based on the bend angle assignments in Figure 3, only the vertices with a positive bend angle can be a corner. The nine points were detected according to the following rules:

1. Vertices with a negative angle will be removed.
2. If there are two adjacent vertices and both with a positive bend angle, the vertex with the smaller bend angle will be removed.
3. There will be total four points left if the shape is close to a rectangle with only minor contour variations. In some cases, vertices with a small positive bend angle are preserved because their adjacent vertices have a negative bend angle. If there are more than four points left, repeat Steps 1 and 2 until only four significant vertices left, which should be the lower or upper corners.
4. Points 2, 5 and 7 are the median along the edge in the sagittal view. The sagittal view means if we draw a straight line between two corners, the median is the point along the edge which has the smallest distance to the mid point of the straight line.
5. Seven points have been found. Bend angle of each of the seven points will be calculated. By checking whether the bend angles of Points 2, 5 and 7 are greater than a threshold, the decision of whether osteophyte(s) are present can be made.
6. If osteophyte(s) are present, then the shape contour should contain Points 8 and/or 9. Actually, Points 8 and/or 9 have already been found in Step 3 as the corners of the overall shape. So, the next task is to locate Points 3 and/or 6. Points 3 and 6 are among 20 points that we start with since they are also the significant points which have a sufficiently large bend angle to remain among the final 20 points.
7. Going back to the final 20 points from curve evolution, the points next to the corners which have a sufficiently large bend angle can be selected as Points 3 and 6. If Points 3 and/or 6 are selected due to the contribution of Points 2 and/or 5, they will be verified by calculating

the bend angle again. The bend angle of Point 3 is the angle formed by connecting Points 8 and 3 and 1 while the bend angle of Point 6 is the one connecting Points 9, 6 and 4. Both of them should be larger than a pre-selected threshold in order to be selected as Points 3 and 6.

Figure 4 shows the result of applying these rules to the 20 points from the curve evolution output. The crosses represent the points marked by the radiologist and the circles represent the selection made by the algorithms.

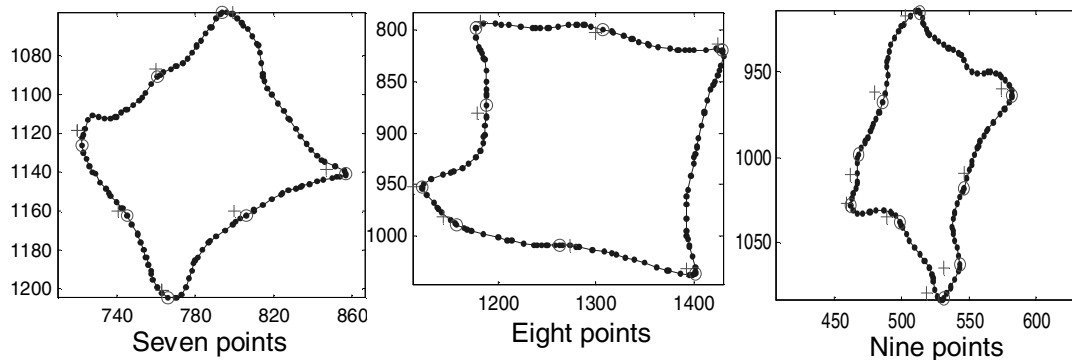


Figure 4. Samples of processing results

3. Performance evaluation

3.1. L_2 distance

There are total 250 expert-marked shapes with associated 7, 8, or 9 points in our database. As mentioned above, shape extraction of x-ray images is a challenging task due to low image contrast. Since the expert selected the nine points by examining x-ray images instead of the shape contours, the image segmentation inaccuracy may cause the loss of key shape features. By checking how the x-ray images align with the segmented contours, we relinquished those contours which lose the key shape features. We selected 197 out of 250 shapes to test the performance of our algorithms by calculating absolute L_2 distance and the minimum L_2 distance. Among the 197 shapes we used, there were 114 shapes with 7 points, 39 shapes with 8 points, and 43 shapes with 9 points. To avoid bias introduced by using the sum of individual L_2 distances on shapes with a variable number (7, 8 or 9) of marked points, the average of L_2 distances is considered more appropriate for comparison. The average L_2 distance of all points is calculated as follows:

$$D = \frac{1}{n} \sum_{j=1}^n \sqrt{(x_j - x'_j)^2 + (y_j - y'_j)^2} \quad \text{Equation 2}$$

And the average minimum L_2 distance is calculated in Equation 3 to minimize effect of the overall contour shift caused by image segmentation.

$$\text{Min}_- D = \frac{1}{n} \sum_{j=1}^n \sqrt{(x_j - x'_j - \delta_x)^2 + (y_j - y'_j - \delta_y)^2} \quad \text{Equation 3}$$

, where n is equal to 7, 8, or 9 depending on how many points the expert picked for each individual x-ray image. The overall contour shift, δ_x and δ_y , are obtained by taking the derivatives of $\text{Min}_- D$ w.r.t δ_x and δ_y separately and setting the derivative to zero. By applying the calculated shift δ_x and δ_y , we minimized the effect of the shift between the original x-ray

image and the segmented shape contour. Although shapes that do not possess the key shape features were excluded from the test, the inaccuracy in image segmentation still has impact on *Min_D*.

Table 1 shows the comparison between *D* and *Min_D* of a few sampled shapes, both expressed in pixels. The difference between the two represents the overall shift. The average *D* of 197 shapes is 12.8415 while the average *Min_D* is 10.6240.

Table 1. The comparison between *D* and *Min_D* of a few samples

| Shape Index | 1 | 4 | 22 | 68 | 117 | 119 | 182 | 183 |
|--------------|--------|--------|---------|---------|---------|--------|--------|---------|
| <i>D</i> | 8.4341 | 5.3689 | 11.0767 | 14.1777 | 21.0441 | 6.191 | 6.8872 | 12.9497 |
| <i>Min_D</i> | 3.5222 | 5.1134 | 7.4792 | 11.5854 | 11.1038 | 3.4198 | 6.537 | 10.341 |

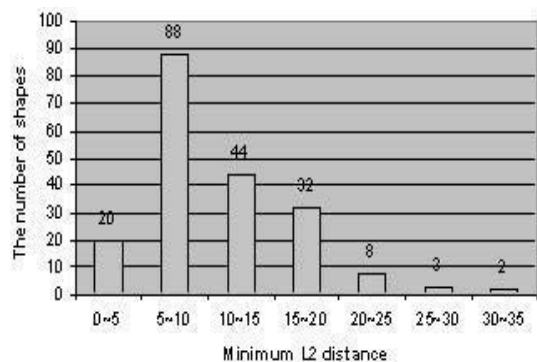


Figure 5. Distribution of *Min_D*

We sampled the *Min_D* of 197 shapes into 7 regions. From the histogram shown in Figure 5, 54% of the 197 shapes' *Min_D* is below 10 pixels; 77% is below 15 pixels and 93% is below 20 pixels. In measuring the L2 norm, it showed that the 9-point selection algorithm worked very well. The results shown in Figure 4 indicate that the relative relation between the two 9-point models is very close. By comparing the L2 distances and the relative relation between the two 9-point models, it shows that the automatic 9-point algorithm works very well.

3.2. Shape indexing based on Fourier Descriptors (FD)

Both the selected 9-point model and the expert marked 9-point model were then used for image indexing and their similarity rankings were compared to evaluate the performance. Shape indexing methods for content-based retrieval of x-ray images have been evaluated [3]. We applied FD to perform the ranking using the two 9-point models. FD of the bend angle function versus the normalized length (*t*) were calculated to provide the translation, rotation, and scaling invariance. The starting point shift invariance requirement is taken care of by the shift invariance property of the power spectrum. This similarity measure meets all the invariance requirements for shape-based retrieval. The lower the difference between two sets of FD, the greater is the similarity between the shapes. This method calculates the FD of a closed polygon curve *C* as $\theta(t)$ and it is expressed as:

$$\theta(t) = \mu_0 + \sum_{n=1}^{\infty} (a_n \cos nt + b_n \sin nt) \quad \text{Equation 4}$$

, where a_n and b_n are coefficients for each frequency component.

Each one of the 197 shapes was used as the query and the rest of 196 shapes were ranked according to their similarity to the query shape. This ranking process was performed for both 9-point models (selected by the algorithm and marked by the expert). Among the 197 shapes we used, there were 104 cervical shapes and 93 lumbar shapes. FD ranked them so distinctly that a lumbar shape could never be mistaken as a cervical shape and vice versa. It means these two groups can be easily separated without confusions.

We compared the indexing result using the two 9-point models in two ways. The shape similarity ranking using the expert-marked 9-point model was used as the reference list. The first comparison was done by counting how many shapes ranked as top 25 on the reference list are also ranked as top 25 on the test list. The other way was to actually measure how well they match. For this purpose, we calculated the total ranking displacement as the summation of the ranking differences. For example, if one shape is found as #1 on the reference list and #4 on the test list, then the ranking difference for that shape was counted as 3. For those shapes that cannot find a match on both lists, the ranking difference was assigned based on their ranks on the reference list. The higher they are on the reference list, the higher ranking difference they will be assigned. Table 2 shows the tests for finding the top 25, 30, 35, and 40 rankings. For example, of the top 25 (or 30) shapes on the reference list, 14 (or 18) of them were also found as top 25 (or 30) on the test list. The average # of shapes matched is the average of 197 queries. The average displacement is the average displacement for each shape on the ranking list.

Table 2. Matching results

| Number of top rankings | 25 | 30 | 35 | 40 |
|-----------------------------|------|------|------|------|
| Average # of shapes matched | 14 | 18 | 23 | 28 |
| Highest # of shapes matched | 22 | 26 | 31 | 36 |
| Average displacement (+/-) | 7.23 | 7.97 | 8.55 | 8.99 |

4. Conclusions

From Table 2, we conclude that the algorithm is able to find the 9 points closely match with the 9 points the expert marked. Since the 9 points are selected based on the shape contours from image segmentation while the marked 9 points are based on x-ray images, there is an inevitable inaccuracy caused by the displacement between the shape contours and the x-ray images. By excluding those shape contours that do not possess key shape features from the data sample, we are able to show that the automatic 9-point selection algorithm can accurately locate the 9 points that provide sufficient information for diagnosis.

5. References

- [1] D.J. Lee, S. Antani, L. R. Long, "Similarity Measurement Using Polygon Curve Representation and Fourier Descriptors for Shape-based Vertebral Image Retrieval," SPIE Medical Imaging, Image Processing, vol. 5032, San Diego, California, USA, February 2003.
- [2] L.R. Long, S., Antani, D.J. Lee, D. Krainak, G.R. Thoma, "Biomedical Information from a National Collection of Spine X-rays: Film to Content-based Retrieval", SPIE Medical Imaging, PACS and Integrated Medical Information Systems: Design and Evaluation, vol. 5033, San Diego, California, USA, February 2003.
- [3] S. Antani, L.R. Long, G.R. Thoma, and D.J. Lee, "Evaluation of Shape Indexing Methods for Content-Based Retrieval of X-Ray Images", SPIE Electronic Imaging, Storage and Retrieval for Media Databases, vol. 5021, Santa Clara, California, USA, January 2003, pp. 405-416.
- [4] L. G. Brown, "A survey of image registration techniques", ACM computing surveys, December 1992, vol. 24, no. 4, pp. 325-376.
- [5] M. Jergas and R. S. Valentin, "Techniques for the Assessment of Vertebral Dimensions in Quantitative Morphometry", Ch. 10, Vertebral Fracture in Osteoporosis, H. K. Genant, M. Jeras, C. van Kuijk, eds. University of California Printing Services. 1995, pp. 163-188.
- [6] M. Kass, A. Witkin, and D. Terzopoulos, "Snakes: Active contour models", International Journal of Computer Vision. 1(4), 1988, pp. 321-331.
- [7] S. Antani, L.R. Long, G. Thoma, "A Biomedical Information System for Combined Content-based Retrieval of Spine X-ray Images and Associated Text Information", Proceedings of the 3rd Indian Conference on Computer Vision Graphics and Image Processing 2002, pp. 242-247.
- [8] D. M. Wuescher and K. L. Boyer, "Robust contour decomposition using a constant curvature criterion", IEEE Transactions on Pattern Analysis and Machine Intelligence, vol. 13, no.1, pp. 41-51.
- [9] A. K. Mackworth and F. Mokhtarian, "The renormalized curvature scale space and the evolution properties of planar curves", Proceedings of IEEE Computer Society Conference on Computer Vision and Pattern Recognition, 5-9 Jun 1988, pp. 318-326.